

# HYPERSPECTRAL IMAGE RESTORATION BY HYBRID SPATIO-SPECTRAL TOTAL VARIATION

Saori Takeyama<sup>†</sup>, Shunsuke Ono<sup>†</sup>, and Itsuo Kumazawa<sup>†</sup>

<sup>†</sup>Tokyo Institute of Technology

## ABSTRACT

We propose a new regularization technique, named *Hybrid Spatio-Spectral Total Variation* (HSSTV), for hyperspectral image (HSI) restoration. Popular regularization techniques for HSIs are total variation functions (TV), and there have been proposed a variety of TVs for HSI restoration. However, they do not *fully* exploit both spatial and spectral smoothness, which are the underlying properties of HSIs, and/or they result in computationally expensive optimization. Our proposed HSSTV is designed to evaluate the two properties via two types of discrete differences of an HSI, leading to much more effective regularization than existing TVs for HSI restoration. HSSTV is defined with local discrete difference operators and the  $\ell_1$ /mixed  $\ell_{1,2}$  norm, so that optimization problems involving it can be efficiently solved by proximal splitting methods, such as the so-called alternating direction method of multipliers. Experimental results illustrate the advantages of HSSTV over state-of-the-art methods.

**Index Terms**— Hyperspectral image restoration, total variation, ADMM

## 1. INTRODUCTION

Hyperspectral imaging has been a very active research topic and offers many applications in a wide range of fields, spanning from remote sensing, geoscience and astronomy to biomedical imaging and signal processing [1, 2]. This is because the very nature of a hyperspectral image (HSI), which consists of a 3D datacube with 2D spatial and 1D spectral variation, reveals the intrinsic characteristics of scene objects and environmental lighting.

Capturing such *rich* spatio-spectral information itself is a challenging task: various types of noise and other effects (e.g., blur and/or missing entries) are inevitable through imaging process, so that one needs to restore a clean HSI from such a degraded observation. In addition, much attention has been paid to one-shot hyperspectral imaging based on the compressed sensing frameworks [3, 4] for its acquisition efficiency, and it inherently requires to estimate a full HSI from incomplete measurements. The said problems have been tackled by *variational approaches* that characterize a restored HSI as a solution of some optimization problems, where *regularization*, modeling a priori knowledge about underlying properties on HSIs, plays an important role to obtain a reasonable result under such ill-posed or ill-conditioned scenarios.

A successful class of regularization techniques for HSIs would be total variation functions (TV), which relies on the spatial smoothness of HSIs, i.e., the total magnitude of local spatial differences is small in HSIs. A popular one is the *hyperspectral TV* (HTV) [5]<sup>1</sup>,

<sup>1</sup>The work was partially supported by JSPS Grants-in-Aid (15H06197, 16K12457, 16H04362) and JST-PRESTO.

<sup>1</sup>HTV can be seen as a generalization of the standard color TV [6]

and more sophisticated versions leveraging semilocal/nonlocal information are also studied [7–9]. However, these TVs do not exploit *spectral smoothness*, another inherent property of HSIs. A recently proposed one [10] considers the spectral smoothness, yielding a powerful regularization technique for color images and HSIs, but this TV requires high computational cost in optimization (mainly due to singular value decomposition), which is a serious issue in HSI restoration due to the high-dimensional nature of HSIs (this is also the case with [7–9]).

Very recently, the *spatio-spectral total variation* (SSTV) [11] is proposed for HSI denoising, which considers spectral smoothness together with spatial smoothness. Specifically, in the definition of SSTV, the local spectral differences of an HSI are calculated before the calculation of the local spatial differences (Fig.1, yellow lines). As a result, SSTV is an effective (considering the spatio-spectral smoothness) and computationally efficient (only exploiting local information) regularization technique for HSIs, as outperforming several popular regularization methods that are not limited to TVs [5, 12–14]. On the other hand, it is clear from the calculation of the discrete differences in SSTV that SSTV does not “directly” evaluate the spatial smoothness of HSIs, so that it often causes undesirable noise-like effects (see Fig. 3).

Based on the above discussion, we propose a new total variation for HSI restoration, termed as *Hybrid Spatio-Spectral Total Variation* (HSSTV). As will be explained in Sec. 2.1, HSSTV is designed to evaluate both the direct spatial smoothness and the spatio-spectral smoothness of HSIs in a unified manner. Therefore, it resolves the drawback of SSTV while keeping its ability, leading to much better regularization. In addition, HSSTV is defined with local discrete differences and the  $\ell_1$ /mixed  $\ell_{1,2}$  norm, as in the case of HTV and SSTV, so that it can be efficiently dealt with by optimization methods based on proximal splitting, such as the alternating direction method of multipliers (ADMM) [15–17]. Experiments on denoising and compressed sensing reconstruction demonstrate the advantages of HSSTV over several state-of-the-art methods.

## 2. PROPOSED METHOD

### 2.1. Hybrid spatio-spectral total variation

Let  $\mathbf{u} \in \mathbb{R}^{NB}$  be a HSI with  $N$  pixels and  $B$  spectral bands, and  $\mathbf{D}_v$ ,  $\mathbf{D}_h$ , and  $\mathbf{D}_b$  are vertical, horizontal, and spectral difference operators, respectively. Furthermore, we define a spatial difference operator as  $\mathbf{D} = (\mathbf{D}_v^T \ \mathbf{D}_h^T)^T \in \mathbb{R}^{2NB \times NB}$ . To exploit both the direct spatial smoothness and the spatio-spectral smoothness of HSIs, we propose a new TV for HSIs as follows:

$$\text{HSSTV}(\mathbf{u}) := \left\| \begin{pmatrix} \mathbf{D}\mathbf{D}_b\mathbf{u} \\ \omega\mathbf{D}\mathbf{u} \end{pmatrix} \right\|_{1,p}, \quad (1)$$

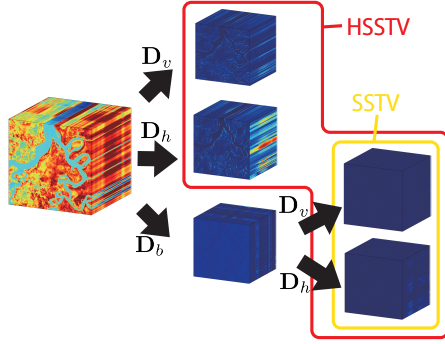


**Fig. 1.** Calculation of local discrete differences in SSTV and the proposed HSSTV. SSTV evaluates the  $\ell_1$  norm of the spatio-spectral differences (yellow lines). HSSTV evaluates the mixed  $\ell_{1,p}$  norm of both the direct spatial and the spatio-spectral differences (red lines).

where  $\|\cdot\|_{1,p}$  is the mixed  $\ell_{1,p}$  norm with  $p = 1$  or  $2$  (NOTE:  $\|\cdot\|_{1,1}$  means the  $\ell_1$  norm), and  $\omega \geq 0$ . Following the prior work [11], we name this function as the *Hybrid Spatio-Spectral Total Variation* (HSSTV). Clearly, HSSTV is a convex function. In the definition of HSSTV,  $\mathbf{D}\mathbf{D}_b\mathbf{u}$  and  $\mathbf{D}\mathbf{u}$  correspond to the local spatio-spectral differences and the local (direct) spatial differences, respectively, as shown in Fig. 1 (red lines), and  $\omega$  controls the relative importance of the direct spatial smoothness to the spatio-spectral smoothness. HSSTV evaluates these two kinds of smoothness by taking the  $\ell_p$  norm ( $p = 1$  or  $2$ ) of four differences associated with each component, and then summing up for all components, so that it can be defined through the mixed  $\ell_{1,p}$  norm. When we set  $\omega = 0$  and  $p = 1$ , HSSTV recovers SSTV. Hence, HSSTV can be seen as a generalization of SSTV.

We remark that the design of HSSTV involving the direct spatial differences is intended to suppress noise-like artifacts that are produced by only imposing the spatio-spectral smoothness, i.e.,  $\omega\mathbf{D}\mathbf{u}$  is supplemental to  $\mathbf{D}\mathbf{D}_b\mathbf{u}$ . In addition, as can be seen in the results of HTV (Fig. 3), imposing the direct spatial smoothness strongly on a restored HSI would cause oversmoothing of the detailed structures. Thus, the weight  $\omega$  should be set to less than one. Indeed, we will empirically show that a good choice of  $\omega$  is around 0.05 to 0.1 for various HSIs.

## 2.2. HSI restoration by HSSTV

### 2.2.1. Problem formulation

Consider to restore an original HSI  $\bar{\mathbf{u}} \in \mathbb{R}^{NB}$  from an observation  $\mathbf{v} \in \mathbb{R}^M$ , which is cast as inverse problems of the form:

$$\mathbf{v} = \Phi\bar{\mathbf{u}} + \mathbf{n},$$

where  $\Phi \in \mathbb{R}^{M \times NB}$  ( $M \leq NB$ ) is a matrix representing a linear observation process (e.g., blur and/or random sampling), and  $\mathbf{n}$  is an additive white Gaussian noise.<sup>2</sup>

Based on the above model, we formulate HSI restoration by HSSTV as the following constrained convex optimization problem:

$$\begin{aligned} \min_{\mathbf{u}} \text{HSSTV}(\mathbf{u}) \\ \text{s.t. } \begin{cases} \Phi\mathbf{u} \in \mathcal{B}_{\mathbf{v},\varepsilon} := \{\mathbf{x} \in \mathbb{R}^M \mid \|\mathbf{x} - \mathbf{v}\| \leq \varepsilon\}, \\ \mathbf{u} \in [\mu_{\min}, \mu_{\max}]^{NB}. \end{cases} \end{aligned} \quad (2)$$

<sup>2</sup>In this paper, we mainly consider Gaussian noise cases but HSSTV can be used in other noise cases, e.g., Poisson and sparse noises, together with suitable data-fidelity measures.

The first constraint in (2) serves as data-fidelity to the observation  $\mathbf{v}$  and it is defined as the  $\mathbf{v}$ -centered  $\ell_2$ -norm ball with the radius  $\varepsilon > 0$ . As mentioned in [18–21], such a constraint-type formulation facilitates the parameter setting because  $\varepsilon$  has a clear meaning. The second constraint in (2) represents the dynamic range of  $\mathbf{u}$  with  $\mu_{\min} < \mu_{\max}$ . Both constraints are closed convex sets, so that Prob. (2) is a convex optimization problem.

### 2.2.2. Optimization

Since Prob. (2) is a convex but highly nonsmooth optimization problem, a suitable iterative algorithm is required to solve it. In this paper, we adopt ADMM [15–17]. It can solve convex optimization problems of the form:

$$\min_{\mathbf{u}, \mathbf{z}} f(\mathbf{u}) + g(\mathbf{z}) \text{ s.t. } \mathbf{z} = \mathbf{G}\mathbf{u}, \quad (3)$$

where  $f$  and  $g$  are proper lower semicontinuous convex functions, and  $\mathbf{G}$  is a full column rank matrix. Here we assume that  $f$  is quadratic and that  $g$  is *proximable*, i.e., the proximity operator<sup>3</sup> [22] of  $g$  is computable. For any  $\mathbf{z}^{(0)}, \mathbf{d}^{(0)}$ , the algorithm of ADMM is given by

$$\begin{cases} \mathbf{u}^{(n+1)} = \arg\min_{\mathbf{u}} f(\mathbf{u}) + \frac{1}{2\gamma} \|\mathbf{z}^{(n)} - \mathbf{G}\mathbf{u} - \mathbf{d}^{(n)}\|^2, \\ \mathbf{z}^{(n+1)} = \text{prox}_{\gamma g}(\mathbf{G}\mathbf{u}^{(n+1)} + \mathbf{d}^{(n)}), \\ \mathbf{d}^{(n+1)} = \mathbf{d}^{(n)} + \mathbf{G}\mathbf{u}^{(n+1)} - \mathbf{z}^{(n+1)}, \end{cases}$$

where  $\gamma > 0$  is a step size of ADMM. In what follows, we reformulate Prob. (2) into Prob. (3) to solve it by ADMM.

First, for notational convenience, we define the operator  $\mathbf{A}_\omega$  by

$$\mathbf{A}_\omega := \begin{pmatrix} \mathbf{D}\mathbf{D}_b \\ \omega\mathbf{D} \end{pmatrix}.$$

Then, we can express HSSTV as

$$\text{HSSTV}(\mathbf{u}) = \|\mathbf{A}_\omega\mathbf{u}\|_{1,p}.$$

Second, by introducing the indicator functions<sup>4</sup> of  $[\mu_{\min}, \mu_{\max}]^{NB}$  and  $\mathcal{B}_{\mathbf{v},\varepsilon}$ , Prob (2) can be rewritten as

$$\min_{\mathbf{u}} \|\mathbf{A}_\omega\mathbf{u}\|_{1,p} + \iota_{\mathcal{B}_{\mathbf{v},\varepsilon}}(\Phi\mathbf{u}) + \iota_{[\mu_{\min}, \mu_{\max}]^{NB}}(\mathbf{u}). \quad (4)$$

Finally, by letting

$$\begin{aligned} f &: \mathbb{R}^{NB} \rightarrow \mathbb{R} : \mathbf{u} \mapsto 0, \\ g &: \mathbb{R}^{5NB+M} \rightarrow \mathbb{R} \cup \{\infty\} : \\ &(\mathbf{z}_1, \mathbf{z}_2, \mathbf{z}_3) \mapsto \|\mathbf{z}_1\|_{1,p} + \iota_{\mathcal{B}_{\mathbf{v},\varepsilon}}(\mathbf{z}_2) + \iota_{[\mu_{\min}, \mu_{\max}]^{NB}}(\mathbf{z}_3), \\ \mathbf{G} &: \mathbb{R}^{NB} \rightarrow \mathbb{R}^{5NB+M} : \mathbf{u} \mapsto (\mathbf{A}_\omega\mathbf{u}, \Phi\mathbf{u}, \mathbf{u}), \end{aligned} \quad (5)$$

Prob. (4) is reduced to Prob. (3). The resulting algorithm based on ADMM is summarized in Alg. 1.

Since the update of  $\mathbf{u}$  in Alg. 1 is strictly-convex quadratic minimization, it boils down to solving the matrix inversion:

$$\begin{aligned} \mathbf{u}^{(n+1)} &= (\mathbf{A}_\omega^\top \mathbf{A}_\omega + \Phi^\top \Phi + \mathbf{I})^{-1} \text{RHS} \\ \text{RHS} &:= (\mathbf{A}_\omega^\top (\mathbf{z}_1^{(n)} - \mathbf{d}_1^{(n)}) + \Phi^\top (\mathbf{z}_2^{(n)} - \mathbf{d}_2^{(n)}) + (\mathbf{z}_3^{(n)} - \mathbf{d}_3^{(n)})). \end{aligned} \quad (7)$$

<sup>3</sup>The proximity operator of index  $\gamma > 0$  of a proper lower semicontinuous convex function  $f$  is defined by  $\text{prox}_{\gamma f}(\mathbf{x}) := \arg\min_{\mathbf{y}} f(\mathbf{y}) + \frac{1}{2\gamma} \|\mathbf{y} - \mathbf{x}\|^2$ .

<sup>4</sup>The indicator function of a nonempty closed convex set  $C$  is defined by  $\iota_C(\mathbf{x}) := 0$ , if  $\mathbf{x} \in C$ ;  $\iota_C(\mathbf{x}) := \infty$ , otherwise.

If  $\Phi$  is a block-circulant-with-circulant-blocks matrix [23], we can leverage 3DFFT to efficiently solve the inversion in (7) with the discrete difference operators having periodic boundary, i.e.,  $\mathbf{A}_\omega^\top \mathbf{A}_\omega + \Phi^\top \Phi + \mathbf{I}$  can be diagonalized by the 3D discrete Fourier transform and its inverse. If  $\Phi$  is a semi-orthogonal matrix, i.e.,  $\Phi \Phi^\top = \alpha \mathbf{I}$  ( $\alpha > 0$ ), we leave it to the update of  $\mathbf{z}_2$ , which means that we replace  $\iota_{\mathcal{B}_{\mathbf{v},\varepsilon}}$  by  $\iota_{\mathcal{B}_{\mathbf{v},\varepsilon}} \circ \Phi$  in (5) and  $\Phi \mathbf{u}$  by  $\mathbf{u}$  in (6). This is because the composition of such a matrix with a proximable function also becomes proximable, see (8). If  $\Phi$  is a sparse matrix, we offer to use a preconditioned conjugate gradient method [24] for approximately solving the inversion, or to apply primal-dual splitting methods [25–27] instead of ADMM.<sup>5</sup> Otherwise, an image restoration method using a stochastic variant of ADMM [28] might be useful for reducing the computational cost.

The update of  $\mathbf{z}_1$ , the proximity operator of the mixed  $\ell_{1,p}$  norm, is reduced to a simple softthresholding type operation: for  $\gamma > 0$  and for  $i = 1, \dots, 4NB$ , (i) in the case of  $p = 1$ ,

$$[\text{prox}_{\gamma \|\cdot\|_1}(\mathbf{x})]_i = \text{sgn}(x_i) \max\{|x_i| - \gamma, 0\},$$

where  $\text{sgn}$  is the sign function, and (ii) in the case of  $p = 2$ ,

$$[\text{prox}_{\gamma \|\cdot\|_{1,2}}(\mathbf{x})]_i = \max\left\{1 - \gamma \left(\sum_{j=0}^3 x_{i+jNB}^2\right)^{-\frac{1}{2}}, 0\right\} x_i,$$

where  $\tilde{i} := ((i-1) \bmod NB) + 1$ .

For the update of  $\mathbf{z}_2$ , since the proximity operator of the indicator function of a nonempty closed convex set  $C$  is equivalent to the metric projection onto  $C$  (i.e.,  $\text{prox}_{\gamma \iota_C} = P_C$ ), the computation of  $\text{prox}_{\gamma \iota_{\mathcal{B}_{\mathbf{v},\varepsilon}}}$  corresponds to calculating the metric projection<sup>6</sup> onto the  $\mathbf{v}$ -centered  $\ell_2$ -norm ball with radius  $\varepsilon$ , given by

$$P_{\mathcal{B}_{\mathbf{v},\varepsilon}}(\mathbf{x}) = \begin{cases} \mathbf{x}, & \text{if } \mathbf{x} \in \mathcal{B}_{\mathbf{v},\varepsilon}, \\ \mathbf{v} + \frac{\varepsilon(\mathbf{x}-\mathbf{v})}{\|\mathbf{x}-\mathbf{v}\|}, & \text{otherwise.} \end{cases}$$

In the case of  $\iota_{\mathcal{B}_{\mathbf{v},\varepsilon}} \circ \Phi$  with  $\Phi$  being semi-orthogonal, i.e.,  $\Phi \Phi^\top = \alpha \mathbf{I}$  ( $\alpha > 0$ ), we can compute its proximity operator by using [29, Table 1.1-x]:

$$\text{prox}_{\gamma \iota_{\mathcal{B}_{\mathbf{v},\varepsilon}} \circ \Phi}(\mathbf{x}) = \mathbf{x} + \alpha^{-1} \Phi^\top (P_{\mathcal{B}_{\mathbf{v},\varepsilon}}(\Phi \mathbf{x}) - \Phi \mathbf{x}). \quad (8)$$

The update of  $\mathbf{z}_3$  also equals to the computation of the metric projection onto the box constraint, i.e., for  $i = 1, \dots, NB$ ,

$$[P[\mu_{\min}, \mu_{\max}]^{NB}(\mathbf{x})]_i = \begin{cases} \mu_{\min}, & \text{if } x_i < \mu_{\min}, \\ \mu_{\max}, & \text{if } x_i > \mu_{\max}, \\ x_i & \text{otherwise.} \end{cases}$$

### 3. EXPERIMENTS

To demonstrate the advantages of HSSTV, we apply it to two specific HSI restoration problems: denoising and compressed sensing (CS) reconstruction, and compare it with HTV [5] and SSTV [11]. In the denoising experiment, we also compare HSSTV with BM4D [30], which is known to be one of the most effective nonlocal denoising methods for 3D signals.

<sup>5</sup>Primal-dual splitting methods require no matrix inversion but in general their convergence speed is slower than ADMM.

<sup>6</sup>Given a vector  $\bar{\mathbf{x}}$  and a nonempty closed convex set  $C$ , the metric projection onto  $C$  is characterized by  $\min_{\mathbf{x} \in C} \|\mathbf{x} - \bar{\mathbf{x}}\|$  s.t.  $\mathbf{x} \in C$ .

#### Algorithm 1: ADMM method for Prob. (2)

---

```

input :  $\mathbf{z}_1^{(0)}, \mathbf{z}_2^{(0)}, \mathbf{z}_3^{(0)}, \mathbf{d}_1^{(0)}, \mathbf{d}_2^{(0)}, \mathbf{d}_3^{(0)}$ 
1 while A stopping criterion is not satisfied do
2    $\mathbf{u}^{(n+1)} = \underset{\mathbf{u}}{\text{argmin}} \frac{1}{2\gamma} (\|\mathbf{z}_1^{(n)} - \mathbf{A}_\omega \mathbf{u} - \mathbf{d}_1^{(n)}\|^2 + \|\mathbf{z}_2^{(n)} - \Phi \mathbf{u} - \mathbf{d}_2^{(n)}\|^2 + \|\mathbf{z}_3^{(n)} - \mathbf{u} - \mathbf{d}_3^{(n)}\|^2);$ 
3    $\mathbf{z}_1^{(n+1)} = \text{prox}_{\gamma \|\cdot\|_{1,p}}(\mathbf{A}_\omega \mathbf{u}^{(n+1)} + \mathbf{d}_1^{(n)});$ 
4    $\mathbf{z}_2^{(n+1)} = \text{prox}_{\gamma \iota_{\mathcal{B}_{\mathbf{v},\varepsilon}}}(\Phi \mathbf{u}^{(n+1)} + \mathbf{d}_2^{(n)});$ 
5    $\mathbf{z}_3^{(n+1)} = \text{prox}_{\gamma \iota_{[\mu_{\min}, \mu_{\max}]^{NB}}}(\mathbf{u}^{(n+1)} + \mathbf{d}_3^{(n)});$ 
6    $\mathbf{d}_1^{(n+1)} = \mathbf{d}_1^{(n)} + \mathbf{A}_\omega \mathbf{u}^{(n+1)} - \mathbf{z}_1^{(n+1)};$ 
7    $\mathbf{d}_2^{(n+1)} = \mathbf{d}_2^{(n)} + \Phi \mathbf{u}^{(n+1)} - \mathbf{z}_2^{(n+1)};$ 
8    $\mathbf{d}_3^{(n+1)} = \mathbf{d}_3^{(n)} + \mathbf{u}^{(n+1)} - \mathbf{z}_3^{(n+1)};$ 
9    $n \leftarrow n + 1;$ 

```

---

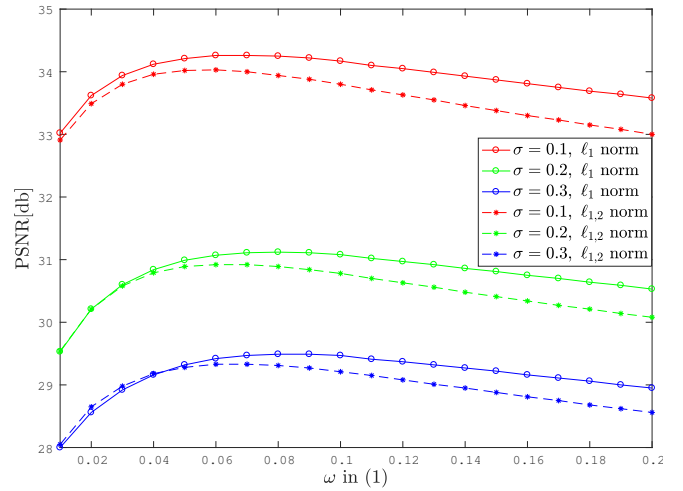


Fig. 2. PSNR versus  $\omega$  in (1) on denoising.

All the experiments were performed using MATLAB (R2016a, 64bit), on a Windows 10 Home (64bit) laptop computer with an Intel Core i7 3.41 GHz processor and 16 GB of RAM. For test HSIs, we took five HSIs from the *SpecTIR* [31] and *MultiSpec* [32], cropped a region of size  $256 \times 256 \times 32$  for each HSI, and normalized their dynamic range into  $[0, 1]$ . We use PSNR [dB] between an original HSI  $\bar{\mathbf{u}}$  and a restored HSI  $\mathbf{u}$ , defined by  $10 \log_{10}(NB/\|\mathbf{u} - \bar{\mathbf{u}}\|^2)$ , for the quantitative evaluation of restored HSIs. We set the max iteration number and the stopping criterion of ADMM to 5000 and  $\|\mathbf{u}^{(n)} - \mathbf{u}^{(n+1)}\| < 0.01$ , respectively.

#### 3.1. Denoising

First, we conducted experiments on Gaussian noise removal, where clean test HSIs were contaminated by an additive white Gaussian noise  $\mathbf{n}$  with the standard deviation  $\sigma$ , i.e.,  $\mathbf{v} = \bar{\mathbf{u}} + \mathbf{n}$ . Specifically, we solve Prob. (2) with  $\Phi = \mathbf{I}$ . For HTV and SSTV, we replace HSSTV in (2) with HTV or SSTV, and solve it by ADMM. For a fair comparison, the radius  $\varepsilon$  in Prob. (2) was set to the oracle value in every method, i.e.,  $\varepsilon = \|\bar{\mathbf{u}} - \mathbf{v}\|$ . For BM4D, we used the program code distributed by the authors of [30].

We show PSNR of denoised HSIs by each method for various  $\sigma$  in the left of Tab. 1, where  $\omega$  in HSSTV is set to 0.08 for the  $\ell_1$  case and 0.06 for the  $\ell_{1,2}$  case. One can see that for all HSIs and  $\sigma$ , HSSTV outperforms HTV and SSTV. Moreover, one also

**Table 1.** PSNR in denoising experiments (left) and CS experiments (right).

	$\sigma$	HTV	SSTV	BM4D	$\ell_1$ -HSSTV	$\ell_{1,2}$ -HSSTV	$\sigma$ and r	HTV	SSTV	$\ell_1$ -HSSTV	$\ell_{1,2}$ -HSSTV
Beltsville	0.1	29.34	31.16	<b>33.39</b>	33.21	32.83	0.1, 0.2	26.23	24.37	<b>29.65</b>	29.19
	0.2	26.94	26.09	30.03	<b>30.31</b>	29.87					
	0.3	25.81	22.89	28.04	<b>28.79</b>	28.38					
Suwannee	0.1	30.05	31.96	34.56	<b>35.29</b>	35.28	0.1, 0.2	26.48	25.70	31.41	<b>31.47</b>
	0.2	27.35	27.58	31.53	32.09	<b>32.15</b>					
	0.3	25.91	24.52	29.79	30.41	<b>30.49</b>					
DC	0.1	26.88	30.99	31.88	<b>32.21</b>	31.78	0.1, 0.2	23.30	24.18	<b>28.00</b>	27.60
	0.2	24.31	25.93	28.27	<b>28.78</b>	28.38					
	0.3	23.07	22.71	26.43	<b>27.00</b>	26.64					
Cuprite	0.1	31.64	32.05	35.65	<b>36.37</b>	36.34	0.1, 0.2	28.78	25.80	<b>33.01</b>	32.99
	0.2	29.35	27.23	32.39	<b>33.48</b>	33.48					
	0.3	28.19	24.54	30.60	31.99	<b>32.01</b>					
Reno	0.1	28.99	31.86	33.44	<b>34.16</b>	33.90	0.1, 0.2	25.56	25.57	<b>30.26</b>	30.06
	0.2	26.51	26.57	29.91	<b>30.94</b>	30.75					
	0.3	25.22	24.48	28.12	<b>29.29</b>	29.14					

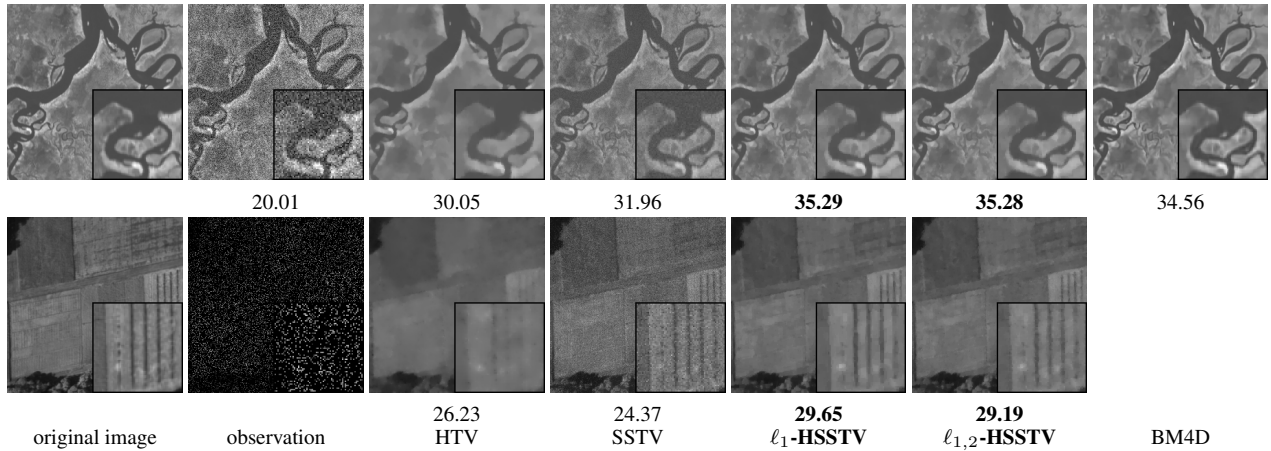


**Fig. 3.** Resulting HSIs with their PSNR on denoising (top, Suwannee) and CS (bottom, Beltsville) experiments.

sees that the denoising ability of HSSTV is better than BM4D for most cases, despite the fact that HSSTV does not exploit nonlocal information. We observe that the performance of SSTV degrades for large  $\sigma$ , which would be due to the absence of evaluating the direct spatial smoothness. Fig. 2 plots PSNR of the denoised HSIs by HSSTV versus  $\omega$  averaged over the five HSIs, which says that  $\omega \in [0.05, 0.1]$  is a good choice in most cases.

Fig. 3 (top) depicts the denoised results on *Suwannee* ( $\sigma = 0.1$ ) with their PSNR. One can see that (i) details are lost in the HSI denoised by HTV, (ii) SSTV cannot remove noise sufficiently, and (iii) HSSTV has a strong ability of detail-preserving denoising.

The average CPU time of one iteration of Alg. 1 (HSSTV with the  $\ell_1$  norm, *Suwannee*) is 0.67 sec, that of ADMM for HTV is 0.24 sec, and that of ADMM for SSTV is 0.31 sec, respectively. Since HSSTV is designed with the  $\ell_1$ /mixed  $\ell_{1,2}$  norm as well as HTV and SSTV, the computation of the associated proximity operator is reduced to a soft-thresholding type operation, which means that the computational cost of using HSSTV is low and is not much different from HTV and SSTV.

### 3.2. Compressed sensing reconstruction

We also conducted experiments on compressed sensing (CS) reconstruction [33, 34], where we try to recover an original HSI from its incomplete measurements. In this case,  $\Phi \in \mathbb{R}^{M \times NB}$  in (2) is a

random sampling matrix ( $M = rNB$  with  $r$  being the rate of random sampling), which is semi-orthogonal (thus we can use (8)). We set  $r = 0.2$  and  $\sigma = 0.1$  (the standard deviation of the additive white Gaussian noise) in the experiments. The radius of the  $\ell_2$ -norm ball was set to  $\varepsilon = \|\Phi \bar{\mathbf{u}} - \mathbf{v}\|$ .

The right of Tab. 1 shows PSNR of reconstructed HSIs. As in the case of denoising, HSSTV leads to much better reconstruction in terms of PSNR than HTV and SSTV.

Fig 3 (bottom) is a showcase of the reconstructed results on *Beltsville*. One can see that (i) HTV causes oversmoothing, (ii) SSTV produces noise-like artifacts, and (iii) HSSTV well reconstructs meaningful details without artifacts.

## 4. CONCLUDING REMARKS

We have proposed a new total variation function (TV) for HSI restoration. Our proposed TV, named the hybrid spatio-spectral total variation (HSSTV), exploits both the direct spatial smoothness and the spatio-spectral smoothness of HSIs. HSI restoration by HSSTV is formulated as a convex optimization problem, and it is efficiently solved by ADMM. Experimental results on denoising and compressed sensing reconstruction demonstrate the effectiveness and utility of HSSTV. Finally, we remark that HSSTV would be able to serve as a building block in a variety of HSI restoration scenarios that are not examined in this paper.

## 5. REFERENCES

- [1] C. I. Chang, *Hyperspectral imaging: techniques for spectral detection and classification*, vol. 1, Springer Science & Business Media, 2003.
- [2] A. Plaza et al., “Recent advances in techniques for hyperspectral image processing,” *Remote sensing of environment*, vol. 113, pp. S110–S122, 2009.
- [3] R. M. Willett, M. F. Duarte, M. A. Davenport, and R. G. Baraniuk, “Sparsity and structure in hyperspectral imaging: Sensing, reconstruction, and target detection,” *IEEE Signal Process. Magazine*, vol. 31, no. 1, pp. 116–126, 2014.
- [4] G. R. Arce, D. J. Brady, L. Carin, H. Arguello, and D. S. Kittle, “Compressive coded aperture spectral imaging: An introduction,” *IEEE Signal Process. Magazine*, vol. 31, no. 1, pp. 105–115, 2014.
- [5] Q. Yuan, L. Zhang, and H. Shen, “Hyperspectral image denoising employing a spectral–spatial adaptive total variation model,” *IEEE Trans. on Geosci. and Remote Sensing*, vol. 50, no. 10, pp. 3660–3677, 2012.
- [6] X. Bresson and T. F. Chan, “Fast dual minimization of the vectorial total variation norm and applications to color image processing,” *Inverse Probl. Imag.*, vol. 2, no. 4, pp. 455–484, 2008.
- [7] S. Lefkimiatis and A. Roussos and P. Maragos and M. Unser, “Structure tensor total variation,” *SIAM J. Imag. Sci.*, vol. 8, no. 2, pp. 1090–1122, 2015.
- [8] S. Lefkimiatis and S. Osher, “Nonlocal structure tensor functionals for image regularization,” *IEEE Trans. Comput. Imag.*, vol. 1, no. 1, pp. 16–29, 2015.
- [9] G. Chierchia, N. Pustelnik, B. Pesquet-Popescu, and J.-C. Pesquet, “A nonlocal structure tensor-based approach for multicomponent image recovery problems,” *IEEE Trans. Image Process.*, vol. 23, no. 12, pp. 5531–5544, 2014.
- [10] S. Ono, K. Shirai, and M. Okuda, “Vectorial total variation based on arranged structure tensor for multichannel image restoration,” in *Proc. IEEE Int. Conf. Acoust., Speech, Signal Process. (ICASSP)*, 2016, pp. 4528–4532.
- [11] H. K. Aggarwal and A. Majumdar, “Hyperspectral image denoising using spatio-spectral total variation,” *IEEE Geosci. and Remote Sens. Lett.*, vol. 13, no. 3, pp. 442–446, 2016.
- [12] G. Chen and S. Qian, “Denoising of hyperspectral imagery using principal component analysis and wavelet shrinkage,” *IEEE Trans. on Geosci. and Remote Sensing*, vol. 49, no. 3, pp. 973–980, 2011.
- [13] H. Zhang, W. He, L. Zhang, H. Shen, and Q. Yuan, “Hyperspectral image restoration using low-rank matrix recovery,” *IEEE Trans. on Geosci. and Remote Sensing*, vol. 52, no. 8, pp. 4729–4743, 2014.
- [14] H. K. Aggarwal and A. Majumdar, “Mixed gaussian and impulse denoising of hyperspectral images,” in *Proc. IEEE Int. Geosci. Remote Sensing Symp. (IGARSS)*, 2015, pp. 429–432.
- [15] D. Gabay and B. Mercier, “A dual algorithm for the solution of nonlinear variational problems via finite elements approximations,” *Comput. Math. Appl.*, vol. 2, pp. 17–40, 1976.
- [16] J. Eckstein and D. P. Bertsekas, “On the Douglas–Rachford splitting method and the proximal point algorithm for maximal monotone operators,” *Math. Program.*, vol. 55, no. 1-3, pp. 293–318, 1992.
- [17] S. Boyd, N. Parikh, E. Chu, B. Peleato, and J. Eckstein, “Distributed optimization and statistical learning via the alternating direction method of multipliers,” *Foundations and Trends in Machine Learning*, vol. 3, no. 1, pp. 1–122, 2011.
- [18] M. Afonso, J. Bioucas-Dias, and M. Figueiredo, “An augmented Lagrangian approach to the constrained optimization formulation of imaging inverse problems,” *IEEE Trans. Image Process.*, vol. 20, no. 3, pp. 681–695, 2011.
- [19] G. Chierchia, N. Pustelnik, J.-C. Pesquet, and B. Pesquet-Popescu, “Epigraphical projection and proximal tools for solving constrained convex optimization problems,” *Signal, Image and Video Process.*, vol. 9, no. 8, pp. 1737–1749, 2015.
- [20] S. Ono and I. Yamada, “Signal recovery with certain involved convex data-fidelity constraints,” *IEEE Trans. Signal Process.*, vol. 63, no. 22, pp. 6149–6163, 2015.
- [21] S. Ono, “ $L_0$  gradient projection,” *IEEE Trans. Image Process.*, 2017, 11 pages, accepted for publication.
- [22] J. J. Moreau, “Fonctions convexes duales et points proximaux dans un espace hilbertien,” *C. R. Acad. Sci. Paris Ser. A Math.*, vol. 255, pp. 2897–2899, 1962.
- [23] P. C. Hansen, J. G. Nagy, and D. P. O’Leary, *Deblurring Images: Matrices, Spectra, and Filtering*, SIAM, 2006.
- [24] G. H. Golub and C. F. Van Loan, *Matrix Computations*, Johns Hopkins University Press, 4th edition, 2012.
- [25] A. Chambolle and T. Pock, “A first-order primal-dual algorithm for convex problems with applications to imaging,” *J. Math. Imaging and Vision*, vol. 40, no. 1, pp. 120–145, 2010.
- [26] P. L. Combettes and J.-C. Pesquet, “Primal-dual splitting algorithm for solving inclusions with mixtures of composite, Lipschitzian, and parallel-sum type monotone operators,” *Set-Valued and Variational Analysis*, vol. 20, no. 2, pp. 307–330, 2012.
- [27] L. Condat, “A primal-dual splitting method for convex optimization involving Lipschitzian, proximable and linear composite terms,” *J. Optimization Theory and Applications*, vol. 158, no. 2, pp. 460–479, 2013.
- [28] S. Ono, M. Yamagishi, T. Miyata, and I. Kumazawa, “Image restoration using a stochastic variant of the alternating direction method of multipliers,” in *Proc. IEEE Int. Conf. Acoust., Speech, Signal Process. (ICASSP)*, 2016, pp. 4523–4527.
- [29] P. L. Combettes and J.-C. Pesquet, “Proximal splitting methods in signal processing,” in *Fixed-Point Algorithms for Inverse Problems in Science and Engineering*, H. H. Bauschke, R. Burachik, P. L. Combettes, V. Elser, D. R. Luke, and H. Wolkowicz, Eds., pp. 185–212. Springer-Verlag, New York, 2011.
- [30] M. Maggioni, V. Katkovnik, K. Egiazarian, and A. Foi, “Nonlocal transform-domain filter for volumetric data denoising and reconstruction,” *IEEE Trans. Image Process.*, vol. 22, no. 1, pp. 119–133, 2013.
- [31] “Spectir,” <http://www.spectir.com/free-data-samples/>.
- [32] “Multispec,” <https://engineering.purdue.edu/biehl/MultiSpec>.
- [33] R. G. Baraniuk, “Compressive sensing,” *IEEE Signal Process. Magazine*, vol. 24, no. 4, 2007.
- [34] E. Candès and M. Wakin, “An introduction to compressive sampling,” *IEEE Signal Process. Magazine*, vol. 25, no. 2, pp. 21–30, 2008.